Extracting Ocean-Generated Tidal Magnetic Signals from Swarm Data through Satellite Gradiometry

Sabaka, Terence J.; Tyler, Robert H.; Olsen, Nils

Published in:
Geophysical Research Letters

Link to article, DOI:
10.1002/2016GL068180

Publication date:
2016

Document Version
Peer reviewed version

Extracting Ocean-Generated Tidal Magnetic Signals from *Swarm* Data through Satellite Gradiometry

Terence J. Sabaka[1], Robert H. Tyler[2], and Nils Olsen[3]

Corresponding author: T. J. Sabaka, Planetary Geodynamics Laboratory, NASA Goddard Space Flight Center, Greenbelt, Maryland, USA. (terence.j.sabaka@nasa.gov)

[1]Planetary Geodynamics Laboratory,

NASA Goddard Space Flight Center,

Greenbelt, Maryland, USA.

[2]Department of Astronomy, University of

Maryland, College Park, Maryland, USA.

[3]DTU Space, National Space Institute,

Technical University of Denmark, Lyngby,

Denmark.

This article has been accepted for publication and undergone full peer review but has not been through the copyediting, typesetting, pagination and proofreading process, which may lead to differences between this version and the Version of Record. Please cite this article as doi: 10.1002/2016GL068180

Ocean-generated magnetic field models of the Principal Lunar, M_2, and the Larger Lunar elliptic, N_2, semi-diurnal tidal constituents were estimated through a "Comprehensive Inversion" of the first 20.5 months of magnetic measurements from ESA's *Swarm* satellite constellation mission. While the constellation provides important north-south along-track gradiometry information, it is the unique low spacecraft pair that allows for east-west cross-track gradiometry. This latter type is crucial in delivering an M_2 estimate of similar quality with that derived from over 10 yrs of CHAMP satellite data, but over a shorter interval, at higher altitude, and during more magnetically disturbed conditions. Recovered N_2 contains non-oceanic signal, but is highly correlated with theoretical models in regions of maximum oceanic amplitude. Thus, satellite magnetic gradiometry may eventually enable the monitoring of ocean electrodynamic properties at temporal resolutions of one to two years, which may have important implications for the inference of ocean temperature and salinity.

Key Points.

- Oceanic M_2 tidal magnetic signal extracted from only 20.5 months of *Swarm* data compared to >3.5 years of CHAMP data.
- *Swarm* gradiometry allows for extraction from higher altitude data compared to CHAMP.
- *Swarm* gradiometry allows for extraction during more magnetically disturbed times compared to CHAMP.

1. Introduction

The spatial gradients of the solar and lunar gravity fields produce ocean tides involving the motion of electrically conducting sea water. In the presence of an ambient main magnetic field, these tides induce electric fields in this moving conductor, which leads to electric currents and resulting magnetic fields. The Principal Lunar semi-diurnal constituent (M_2) represents the tidal gravitational field of the Moon projected onto a circular, equatorial orbit around the Earth. The Larger Lunar elliptic semi-diurnal constituent (N_2) represents the modulation of this tidal force due to the Moon's elliptic orbit about Earth that causes the Earth-Moon distance to oscillate. Additional constituents refine the representation of the solar and lunar gravity field effects. *Tyler et al.* [2003] first showed that ocean-generated magnetic fields could be detected in satellite magnetic measurements by identifying the M_2 tidal signal in early CHAMP satellite data. More recently, *Sabaka et al.* [2015] successfully extracted the M_2 signal from the CHAMP mission in the context of their "Comprehensive Inversion" (CI) approach leading to the CM5 model. In the CI method the major near-Earth magnetic field sources are parameterized and then co-estimated to obtain optimal field separation [see *Sabaka et al.*, 2002, 2004; *Sabaka and Olsen*, 2006]. While CM5 used measured along-track magnetic field vector differences to estimate the high-degree lithospheric field it did not use them for estimating M_2. However, given the strong gradiometric character of the *Swarm* constellation, it was decided to try to estimate the two dominant semi-diurnal oceanic tidal constituents, that is, M_2 (with period T_{M_2}=12.42060122 hr) and N_2 (with period of T_{N_2}=12.65834751 hr) from *Swarm*

along-track and cross-track magnetic field differences from the first 20.5 months of the mission using the CI method.

The *Swarm* mission was launched by the European Space Agency (ESA) on 22 November 2013 and consists of a trio of satellites; a pair of spacecraft flying side-by-side in polar orbits separated by 1.4° in longitude with inclination 87.4° at mean altitudes of about 455 km as of January 2016, and a single satellite at a higher mean altitude of about 515 km as of January 2016 flying in a polar orbit with inclination 88° [*Olsen et al.*, 2015]. Each satellite in this magnetic constellation has an absolute scalar magnetometer (ASM) to measure the magnetic field intensity and a vector fluxgate magnetometer (VFM) to measure the full magnetic field vector. In addition, a triple-head star imager allows for the precise orientation of the field vector with respect to a know reference frame. Thus, all three satellites contribute along-track differences, which are mostly north-south, while the low-pair provide cross-track differences, which are mostly east-west, especially at low-mid latitudes.

It has been demonstrated that lithospheric magnetic field modeling can benefit greatly from the use of magnetic gradient data from satellites. For example, *Kotsiaros et al.* [2015] and *Sabaka et al.* [2015] used along-track magnetic field differences from the CHAMP satellite mission to enhance the recovery of the lithospheric field. The more advanced constellation approach of *Swarm* was designed to provide simultaneous along-track and cross-track gradients to fulfill its lithospheric field science objective [*Friis-Christensen et al.*, 2006], and has in fact produced the *Swarm* Initial Field Model (SIFM) [*Olsen et al.*, 2015]. Magnetic field differencing is useful for two reasons: (1) it amplifies small-

scale structure [*Sabaka et al.*, 2013], and (2) it eliminates large-scale structure, particularly degree-1 external fields mostly due to the rapidly varying magnetospheric ring current, which are manifested as uniform fields in satellite sampling shells. It is this second property that suggests a possible use of gradiometry for extracting the weak signals associated with oceanic tidal motion, which are typically $< 2-3$ nT at satellite altitude. This is a worthy endeavor because time variable magnetic fields can sound Earth's interior, thus providing information about its conductive layers [*Kuvshinov et al.*, 2006; *Kuvshinov and Olsen*, 2006; *Velímsky*, 2010; *Velímský*, 2013; *Püthe et al.*, 2015; *Schnepf et al.*, 2015].

This paper reports on the tidal portion of a model, denoted as "CI1", estimated from *Swarm* magnetic gradiometry measurements using the CI approach and in particular, focuses on the efficacy of using satellite gradiometry to extract ocean-generated signals. Section 2 describes the methodology used to derive the model, that is, the data used and a brief description of the model while Section 3 assesses the quality of the recovery of the M_2 and N_2 tidal constituents and, in the former case, compares this with its recovery from CHAMP satellite data.

2. Methodology

2.1. Data Selection

The data used is from the *Swarm* Level 1b archives and the selection procedure essentially follows that of the SIFM [*Olsen et al.*, 2015] and CHAOS-4 [*Olsen et al.*, 2014] models and includes measurements collected over a 20.5 month span from 28 November 2013 to 15 August 2015 during geomagnetic quiet times. Vector and scalar data are selected when the strength of the magnetospheric ring-current, as measured by the *RC* index [see *Olsen*

et al., 2014], is such that $|dRC/dt|<2$ nT/hr. In non-polar regions, defined as having quasi-dipole (QD) latitudes [see *Richmond*, 1995] equatorward of $\pm 55^\circ$ QD latitude, the geomagnetic activity due to solar particles, as measured by the Kp index [see *Rangarajan*, 1989], must be such that $Kp \leq 2^0$. For polar regions, defined as being poleward of $\pm 55^\circ$ QD latitude, the weighted average over the preceding 1 hr of the merging electric field at the magnetopause [see *Kan and Lee*, 1979; *Newell et al.*, 2007] must be below 0.8 mV/m. Vector and scalar field data are only used in the nightside sector, defined to be the region where the Sun is at least 10° below the horizon, but both scalar and vector along and cross-track differences and complementary sums [see *Sabaka et al.*, 2015] are used at all local times. However, the selection criteria for dayside sums/differences (S/D) data are relaxed to $Kp \leq 3^0$ and $|dRC/dt|<3$ nT/hr in order to include more data. No vector field measurements, including S/D, are used in the polar regions. As with the SIFM model, no gradient data are used in the region between $\pm 10^\circ$ QD latitude on the dayside so as to avoid contamination by the Equatorial Electrojet (EEJ) [*Richmond*, 1973]. Further information on how the vector and scalar data are transformed into S/D pairs may be found in *Olsen et al.* [2015]; *Sabaka et al.* [2013].

In addition to the *Swarm* satellite data, observatory hourly-means (OHM) from 119 stations were also included in the model over the period 1 January 2013 to 16 June 2015. These were taken from the corrected data set described in *Macmillan and Olsen* [2013]. The selection was during geomagnetic quiet times, defined as $Kp \leq 2^0$ and $|dDst/dt|<2$ nT/hr, and at all local times [*Olsen et al.*, 2014]. Here the Dst index [see *Sugiura*, 1964] plays a similar role to that of the RC index.

2.2. Model Construction

The CI1 model development closely follows the procedures discussed in *Sabaka et al.* [2013, 2015] where additional information may be found. Briefly, the model is composed of several different source parameterizations, including:

1. Degree and order (D/O) 90 internal spherical harmonic expansion (SHE) for the core and lithospheric fields.

2. D/O 13 internal SHE linear time dependence (linear secular variation).

3. D/O 1 external SHE for the magnetospheric and associated internal SHE for the induced fields in 1 hr bins.

4. Ionospheric field similar to that of CM5, including accounting for 3-D induction in the Earth's interior via coupling matrices.

5. D/O 36 internal SHE for the M_2 and N_2 tidal fields with appropriate periodic variations identical in form to that used for M_2 by *Sabaka et al.* [2015]. For instance, the M_2 magnetic potential at time rendered from an epoch when the mean Moon position transits the Greenwich meridian, Δt, and at geographic radius, colatitude, and longitude (r, θ, ϕ), denoted by position vector $\mathbf{r}$, is given by

$$V_{M_2}(\Delta t, \mathbf{r}) = \Re\left\{\exp\left(i\omega_{M_2}\Delta t\right) a \sum_{n=1}^{36}\left(\frac{a}{r}\right)^{n+1}\sum_{m=-n}^{n}\tau_n^m Y_n^m(\theta,\phi)\right\}, \tag{1}$$

where $\Re\{\cdot\}$ takes the real part of the expression only, ω_{M_2}=$2\pi/T_{M_2}$ rads/hr is the angular velocity, a is Earth's mean radius (6371.2 km), and τ_n^m is the complex coefficient corresponding to the surface harmonic for degree n and order m

$$Y_n^m(\theta,\phi) = P_n^m(\cos\theta)\exp im\phi, \tag{2}$$

where P_n^m is the Schmidt semi-normalized associated Legendre function. The M_2 magnetic field is then given by $\mathbf{B}_{M_2}(\Delta t, \mathbf{r}) = -\nabla V_{M_2}(\Delta t, \mathbf{r})$. It should be noted that *Sabaka et al.* [2015] used a D/O 36 truncation level to approximate the resolution of the original $5^\circ \times 5^\circ$ block analysis of *Tyler et al.* [2003] and that it is used here for purposes of comparison between CHAMP and *Swarm*.

6. Rotations between the common reference frame of the star imager and the VFM parameterized as 3 Euler angles for each satellite in 10 day bins.

7. Observatory vector bias for each station.

The variance part of the formal error treatment uses uncertainties of 2.2 nT for field and 0.3 nT for S/D data. The CI method employs "Selective Infinite Variance Weighting" (SIVW), introduced in *Sabaka et al.* [2013], for mitigating the bias part of the error such that the data/parameter sensitivity mapping is as follows:

1. Nominal core field (D/O 1−13) determined by all nightside data.

2. Nominal lithospheric field (D/O 14−90) determined by all field and difference data except low-latitude dayside.

3. Ionospheric field determined by all except difference data.

4. Magnetosphere and associated induced determined by all data.

5. Nominal tidal fields determined by all field and difference data except low-latitude dayside.

6. Euler angles determined by all vector data.

Although attitude error is not explicitly treated in this model (since data is only used when at least two star imager heads provide attitude information), Huber weighting [*Hu-*

ber, 2011] is applied in the reference system determined by the star imager boresight and magnetic field directions [*Holme and Bloxham*, 1996; *Sabaka et al.*, 2013] for field data and in the local "North, East, Down" (NED) system for the S/D data.

The total number of parameters, including both nominal and nuisance, is 117,537 and these are estimated in a least-squares sense by applying four Gauss-Newton iterations [*Sorenson*, 1980]. A complete description and assessment of the CI1 model will be reported in a forthcoming publication while the remainder of this paper will focus on its tidal field results.

3. Results and Discussion

3.1. Theoretical Forward Models

It is beneficial to compare the *Swarm* M_2 and N_2 tidal constituents with theoretical forward models. The method and model for simulating the tidal magnetic fields in this study are similar to that of the Tyler simulation used in *Sabaka et al.* [2015]. The model is an extension of *Tyler et al.* [2003], which implements finite differencing and spherical harmonic decomposition to solve an approximate version of the electromagnetic induction equation over a global thin shell comprising the electrically conducting oceans and sediments. In this application, electrical currents are generated by the interaction of the tidal flow (prescribed using TPXO7.2 [*Egbert and Erofeeva*, 2002]) and the ambient main magnetic field (D/O 15 internal SHE) from CM5 at epoch 2007.0 as in *Sabaka et al.* [2015]. However, whereas the previous simulation assumed an insulating upper mantle to provide an end-member estimate, the simulations here include a radially dependent exponential profile with values of 10 S/m at 1000 km depth and 8.0×10^{-3} S/m at the surface

(more specifically, the bottom of the thin conducting shell comprising ocean and sediments). These mantle conductivity parameters fall within the range described in *Püthe et al.* [2015] and are chosen such that the resulting low-degree portion of the M_2 field power spectrum falls between those of the CHAMP estimate of *Sabaka et al.* [2015] and the *Swarm* estimate of this study, thus leading to fairer assessments of both estimates. Including the conductive upper mantle requires numerical solution (rather than analytical solution, as in *Sabaka et al.* [2015]) of an ordinary differential equation representing the radial dependence of the induction equation in the upper mantle. Another difference is that the ocean conductivity used is taken from a recently compiled data set calculated from ocean temperature and salinity observations rather than their climatologies [*Tyler et al.*, 2016]. The method, resolution and other parameters in the M_2 simulation here are identical to those in *Sabaka et al.* [2015]. The method for the N_2 simulation is identical to that of M_2, though with the N_2 tidal flow used instead.

3.2. M_2 Tide

The M_2 tide is the dominant oceanic tidal constituent detectible at satellite altitude [*Tyler et al.*, 2003]. Its parameterization in the CI1 model is identical to that of CM5 where the time-dependent coefficients are sinusoids of the M_2 period T_{M_2}=12.42060122 hr, but no other spatial/temporal information is imposed. The CI1 full-gradiometry *Swarm* results will be compared to five other cases: (1) the theoretical forward model just described, (2) the CHAMP results from the CM5 model [*Sabaka et al.*, 2015], and variants to CI1 in which (3) no north-south gradiometry is used ("NoNSG"), (4) no east-west gradiometry is used ("NoEWG"), and (5) no gradiometry at all is used ("NoG"). It should be noted that in

these final three cases the eliminated gradient data are replaced by the equivalent field data whose dayside portion is subsequently not used in determining the tidal constituent. This is done in order to retain the same basic measurements in each case for fairer comparisons. This is reflected in the satellite measurement counts given in Table 1. Each case also includes 465,747 vector OHM measurements from the ground geomagnetic observatories.

An initial assessment is provided by a comparison of magnetic power in the form of a modification to the $R_n(r)$ spectrum of *Lowes* [1966], which measures the mean-squared magnitude of the M_2 magnetic field, $\mathbf{B}_{M_2}$, over a surface Ω of radius r per spherical harmonic degree n, but now includes a time average over T_{M_2} given by [*Sabaka et al.*, 2015]

$$\frac{1}{4\pi r^2 T_{M_2}} \int_0^{T_{M_2}} \int_\Omega \left|\mathbf{B}_{M_2}(t,\mathbf{r})\right|^2 \, d\Omega \, dt = \sum_{n=1}^{36} R_n(r), \tag{3}$$

where

$$R_n(r) = (n+1)\left(\frac{a}{r}\right)^{2n+4} \left\{ \frac{1}{2}\left|\tau_n^0\right|^2 + \sum_{m=1}^{n} \left[\left|\tau_n^m\right|^2 + \left|\tau_n^{-m}\right|^2 \right] \right\}. \tag{4}$$

For this comparison, $\mathbf{r}$ is the position vector to a sphere of Earth mean radius r=a. Figure 1 shows the R_n spectra with power from all models peaking at degrees n=5−6, but a substantially weaker field from CHAMP. Power from the CHAMP and *Swarm* full-gradiometry models begin to rise beyond n=18 (shown by the vertical dashed line) and this is taken as the truncation level for the trust region. Note that at the highest degrees the *Swarm* model shows less extraneous power. The *Swarm* models with limited gradient data begin to diverge much sooner at about n=9 with the "NoG" case showing the most power. However, it is interesting to see that it appears to be more detrimental when

eliminating east-west, "NoEWG", as opposed to north-south, "NoNSG", gradients, at least with respect to extraneous power.

A comparison based upon spatial patterns is shown in Figure in the form of the amplitude and phase of the radial magnetic component, B_r, of the M_2 fields. From eq. 1 the radial magnetic field at time Δt and position $\mathbf{r}$ is given by

$$B_r(\Delta t, \mathbf{r}) = \Re \left\{ \exp\left(i\omega_{M_2}\Delta t\right)\, \tilde{B}_r(\mathbf{r}) \right\}, \tag{5}$$

where

$$\tilde{B}_r(\mathbf{r}) = \sum_{n=1}^{36}(n+1)\left(\frac{a}{r}\right)^{n+2} \sum_{m=-n}^{n} \tau_n^m Y_n^m(\theta,\phi) \tag{6}$$

is a complex number whose amplitude and argument are the amplitude and phase of B_r. Because of the construction of Δt, this is the Greenwich phase, which measures the angular lag of high tide after the mean Moon's transit over the Greenwich meridian. The maps are generated at an altitude of 430 km for degrees n=1−36. The degrees beyond n=18 were included in order to illustrate the effects of including gradient data. The simulated, CHAMP and *Swarm* full-gradiometry cases appear to agree fairly well with respect to the largest features and many smaller features in both the amplitude and phase maps. The *Swarm* cases with limited gradient data suggest less degradation when excluding north-south gradients as opposed to east-west gradients, not surprisingly in the form of longitudinal striping. Figures 1 and make a strong case for the efficacy of gradiometry data from the *Swarm* constellation in resolving the oceanic M_2 tidal constituent. While north-south gradients can be provided by any single satellite in polar orbit, the apparently crucial east-west gradients can only be provided by the unique orbital design of the *Swarm* low-pair.

To further emphasize the strong performance of the *Swarm* constellation design, Figure shows the altitude of the CHAMP satellite over its ∼10 yr mission lifetime and the mean-altitude of the *Swarm* low-pair over the first 20.5 months of the mission. In addition, the $F_{10.7}$ solar radiation index is also shown on the same plot. These two quantities greatly affect the signal-to-noise ratio of the M_2 signal: (1) because the magnetic field is a potential field, its strength weakens with distance from source, and (2) greater solar activity, as tracked by the $F_{10.7}$ index, causes higher magnetic disturbance levels, which hamper the M_2 recovery. With this in mind, note that in the last ∼3.5 yrs of the CHAMP mission (shown as vertical dashed lines) the altitude was < 350 km and solar activity was $F_{10.7}$<$80 \times 10^{-22}\mathrm{Wm}^{-2}\mathrm{Hz}^{-1}$. These low values provide optimal conditions for the recovery of M_2. In contrast, the mean-altitude of the *Swarm* low-pair was > 450 km while the solar activity was almost twice as high at $F_{10.7}$∼$140 \times 10^{-22}\mathrm{Wm}^{-2}\mathrm{Hz}^{-1}$. Furthermore, the data window for *Swarm* is only 20.5 months. This suggests the possibility of monitoring temporal variations in the magnetic M_2 signal continuously through unfavorable solar conditions. This could be valuable in inferring the associated fluctuations in the ocean electrical conductivity, from which variations in temperature and salinity might be inferred.

3.3. N_2 Tide

The second lunar semi-diurnal constituent co-estimated in CI1 is the N_2 tide with period T_{N_2}=12.65834751 hr. This tidal signal was detected in the power spectrum of CHAMP data over the Indian ocean by *Maus and Kuvshinov* [2004] and is approximately one-quarter of the strength of M_2 at Earth's surface. Figure shows the R_n spectrum of eq. 3

computed from CI1 (red) and the theoretical model of Tyler (green) at Earth's surface. Although the CI1 power is significantly larger than that of the theoretical model, they do have similar local peaks at n=5 and 6 for CI1 and Tyler, respectively, and although the CI1 power begins to ramp up slightly after n=10, the largest excursions begin above n=15 (vertical dashed line) and so this is the truncation level of the CI1 N_2 model used for further comparison.

Figure shows a series of maps of the magnitude of the N_2 tidal magnetic field averaged over its period of T_{N_2}=12.65834751 hr defined at position $\mathbf{r}$ as

$$\overline{|\mathbf{B}_{N_2}(\mathbf{r})|} = \frac{1}{T_{N_2}} \int_0^{T_{N_2}} |\mathbf{B}_{N_2}(t,\mathbf{r})| \; dt. \tag{7}$$

For this comparison, the maps are computed for an altitude of 430 km for degrees n=1−15. Looking at the top row, the maps of Tyler (left column) and CI1 (middle column) indicate that there is evidently much signal in the CI1 model that does not correspond to oceanic sources. Therefore, the CI1 map was redrawn (right column), but only in the regions where its time-averaged correlations, $\rho(\mathbf{r})$, with the Tyler model were above 0.7 as defined by

$$\rho(\mathbf{r}) = \frac{1}{T_{N_2}} \int_0^{T_{N_2}} \frac{\mathbf{B}_1(t,\mathbf{r}) \cdot \mathbf{B}_2(t,\mathbf{r})}{|\mathbf{B}_1(t,\mathbf{r})| \, |\mathbf{B}_2(t,\mathbf{r})|} \; dt, \tag{8}$$

where $\mathbf{B}_1$ and $\mathbf{B}_2$ represent the two N_2 tidal magnetic fields being correlated. Although the magnitudes do not agree particularly well, it is interesting to see that regions where $\rho(\mathbf{r}) > 0.7$ generally correspond to regions of highest magnitude in the oceanic signal of Tyler, such as the Indian and north Atlantic oceans and the area around New Zealand. This suggests that while the oceanic part of the tide may be present in CI1, there are additional sources present.

In order to address this, the N_2 signals from Tyler and CI1 were decomposed into eastward and westward propagating modes, i.e., terms corresponding to negative and positive m, respectively, in eq. 1. The non-propagating modes corresponding to m=0 were distributed equally between those eastward and westward. These are shown in the middle row (eastward) and bottom row (westward) of Figure in the same form as the top row. Most of the extraneous CI1 signal is seen to propagate westward. This may provide useful insight into the nature of the unresolved source as ionospheric currents also show disproportionate energy in their westward propagation at luni-solar frequencies.

4. Conclusions

The M_2 and N_2 tidal constituents have been retrieved from a CI model, denoted CI1, based upon the first 20.5 months of *Swarm* satellite data. Comparisons with theoretical tidal simulation models, and in the case of M_2, the CM5 model based upon CHAMP data, show the efficacy of the *Swarm* constellation design in delivering gradiometry information that can be used in successfully extracting these tides. This is noteworthy since the 20.5 month interval is significantly shorter than the >10 yr CHAMP mission, which includes the ∼3.5 yr optimal window of low-altitude and low solar activity at the end of the mission. Comparisons also show that the unique east-west cross-track differences between the *Swarm* spacecraft low-pair are more important in eliminating extraneous signal than the along-track north-south differences with regard to the oceanic M_2 field. It should be noted that the orbital planes of the high versus the low-pair *Swarm* satellites are not expected to be maximally separated until ∼4 yrs into the mission and this 90° orbital plane configuration is the best for separation of external fields. It is therefore

likely that even better models can be made over an 18−24 month window as the mission progresses, which allows for a higher rate of sampling of the electrodynamic properties of the ocean.

Although the weaker N_2 tidal constituent of CI1 appears to contain significant signal from sources other than the ocean, point-wise correlations with a theoretical forward model provide some confidence that the models are more similar in regions of maximum oceanic N_2 signal strength. A decomposition of the signal into eastward and westward propagating modes indicates that the westward modes have more energy, which is in keeping with solar-fixed sources in the ionosphere. Future work will focus on using such anomalies to better separate the oceanic from external sources for all tidal constituents.

Through its unique configuration, the *Swarm* mission is providing unprecedented types of observations that can be used for the separation of various magnetic field sources, and when combined with the CI approach this makes for a powerful analysis tool. As the mission progresses it is expected that additional data will help in deriving even better tidal models, not only for M_2, but for other constituents like N_2 and the major diurnal modes K_1 and O_1. These tidal models are available to the community by contacting the authors directly.

Acknowledgments. We would like to thank ESA for access to the *Swarm* Level 1b data. We would also like to thank the staff of the geomagnetic observatories and INTERMAGNET for supplying high-quality observatory data. We thank two anonymous reviewers for their valuable comments and we thank Richard Ray for useful discussions and for providing Greenwich phase calculation software. Several figures were generated

using the Generic Mapping Tools (GMT) package [*Wessel and Smith*, 1991]. The NASA Center for Climate Simulation at Goddard Space Flight Center provided computational resources. TJS and RHT are supported by the NASA Earth Surface and Interior program, and NiO is supported by ESA's STSE program. Swarm Level 1b data are available from ESA at http://earth.esa.int/swarm and the tidal coefficients of CI1 are available by contacting the authors directly.

References

Egbert, G., and S. Erofeeva (2002), Efficient inverse modelling of barotropic ocean tides, *J. Ocean. Atmosph. Technol.*, *19*, 183–204.

Friis-Christensen, E., H. Lühr, and G. Hulot (2006), *Swarm*: A constellation to study the Earth's magnetic field, *Earth, Planets and Space*, *58*, 351–358.

Holme, R., and J. Bloxham (1996), The treatment of attitude errors in satellite geomagnetic data, *Phys. Earth Planet. Int.*, *98*, 221–233.

Huber, P. J. (2011), *Robust statistics*, Springer.

Kan, J. R., and L. C. Lee (1979), Energy coupling function and solar wind-magnetosphere dynamo, *Geophys. Res. Lett.*, *6*, 577–580.

Kotsiaros, S., C. C. Finlay, and N. Olsen (2015), Use of along-track magnetic field differences in lithospheric field modelling, *Geophys. J. Int.*, *200*(2), 878–887, doi: 10.1093/gji/ggu431.

Kuvshinov, A. V., and N. Olsen (2006), A global model of mantle conductivity derived from 5 years of CHAMP, Ørsted, and SAC-C magnetic data, *Geophys. Res. Lett.*, *33*, L18301, doi:10.1029/2006GL027083.

Kuvshinov, A. V., T. J. Sabaka, and N. Olsen (2006), 3-D electromagnetic induction studies using the *Swarm* constellation. Mapping conductivity anomalies in the Earth's mantle, *Earth, Planets and Space*, *58*, 417–427.

Lowes, F. J. (1966), Mean-square values on sphere of spherical harmonic vector fields, *J. Geophys. Res.*, *71*, 2179.

Macmillan, S., and N. Olsen (2013), Observatory data and the Swarm mission, *Earth, Planets and Space*, *65*, 1355–1362.

Maus, S., and A. Kuvshinov (2004), Ocean tidal signals in observatory and satellite magnetic measurements, *Geophys. Res. Lett.*, *31*(L15313), doi:10.1029/2004GL020090.

Newell, P. T., T. Sotirelis, K. Liou, C.-I. Meng, and F. J. Rich (2007), A nearly universal solar wind-magnetosphere coupling function inferred from 10 magnetospheric state variables, *J. Geophys. Res.*, *112*(A1), doi:10.1029/2006JA012015.

Olsen, N., H. Lühr, C. C. Finlay, T. J. Sabaka, I. Michaelis, J. Rauberg, and L. Tøffner-Clausen (2014), The CHAOS-4 Geomagnetic Field Model, *Geophys. J. Int.*, *197*, 815 – 827.

Olsen, N., et al. (2015), The Swarm Initial Field Model for the 2014 geomagnetic field, *Geophys. Res. Lett.*, pp. n/a–n/a, doi:10.1002/2014GL062659, 2014GL062659.

Püthe, C., A. Kuvshinov, A. Khan, and N. Olsen (2015), A new model of earth's radial conductivity structure derived from over 10 yr of satellite and observatory magnetic data, *Geophys. J. Int.*, *203*(3), 1864–1872, doi:10.1093/gji/ggv407.

Rangarajan, G. K. (1989), Indices of geomagnetic activity, in *Geomagnetism*, vol. 3, edited by J. A. Jacobs, pp. 323–384, Academic Press, London.

Richmond, A. D. (1973), Equatorial electrojet, I, *J. Atmos. Terr. Phys.*, *35*, 1082–1103.

Richmond, A. D. (1995), Ionospheric electrodynamics using magnetic Apex coordinates, *J. Geomagn. Geoelectr.*, *47*, 191–212.

Sabaka, T. J., and N. Olsen (2006), Enhancing comprehensive inversions using the *Swarm* constellation, *Earth, Planets and Space*, *58*, 371–395.

Sabaka, T. J., N. Olsen, and R. A. Langel (2002), A comprehensive model of the quiet-time near-Earth magnetic field: Phase 3, *Geophys. J. Int.*, *151*, 32–68.

Sabaka, T. J., N. Olsen, and M. E. Purucker (2004), Extending comprehensive models of the Earth's magnetic field with Ørsted and CHAMP data, *Geophys. J. Int.*, *159*, 521–547, doi:10.1111/j.1365-246X.2004.02421.x.

Sabaka, T. J., L. Tøffner-Clausen, and N. Olsen (2013), Use of the Comprehensive Inversion Method for Swarm satellite data analysis, *Earth, Planets and Space*, *65*, 1201–1222.

Sabaka, T. J., N. Olsen, R. H. Tyler, and A. Kuvshinov (2015), CM5, a pre-*Swarm* comprehensive magnetic field model derived from over 12 years of CHAMP, Ørsted, SAC-C and observatory data, *Geophys. J. Int.*, *200*, 1596–1626, doi:10.1093/gji/ggu493.

Schnepf, N. R., A. Kuvshinov, and T. Sabaka (2015), Can we probe the conductivity of the lithosphere and upper mantle using satellite tidal magnetic signals?, *Geophys. Res. Lett.*, *42*, doi:10.1002/2015GL063540.

Sorenson, H. (1980), *Parameter estimation*, Marcel Dekker, Inc., New York.

Sugiura, M. (1964), Hourly values of equatorial Dst for IGY, *Ann. Int. Geophys. Year*, *35*, 49.

Tyler, R. H., S. Maus, and H. Lühr (2003), Satellite observations of magnetic fields due to ocean tidal flow, *Science*, *299*, 239–241.

Tyler, R. H., T. P. Boyer, T. Minami, M. M. Zweng, and J. R. Reagan (2016), Electrical conductivity of the global ocean, *Earth Planet. Sci. Lett.*, *Submitted*.

Velímsky, J. (2010), Electrical conductivity in the lower mantle: Constraints from CHAMP satellite data by time-domain EM induction modelling, *Phys. Earth Planet. Int.*, *180*(3-4), 111–117, doi:10.1016/j.pepi.2010.02.007.

Velímský, J. (2013), Determination of three-dimensional distribution of electrical conductivity in the Earth's mantle from Swarm satellite data: Time-domain approach, *Earth, Planets and Space*, *65*, 1239–1246.

Wessel, P., and W. H. F. Smith (1991), Free software helps map and display data, *EOS Trans. AGU*, *441*(72), 445–4465.

Table 1. Number of Satellite Vector and Scalar Single and S/D Pair Measurements used in each CI1 Model Variant.

	Full	NoNSG	NoEWG	NoG
Single Vector	564,129	2,448,393	1,549,869	3,434,133
Single Scalar	613,717	3,661,939	2,210,395	5,258,617
S/D Vector Pair	1,435,002	492,870	942,132	0
S/D Scalar Pair	2,322,450	798,339	1,524,111	0

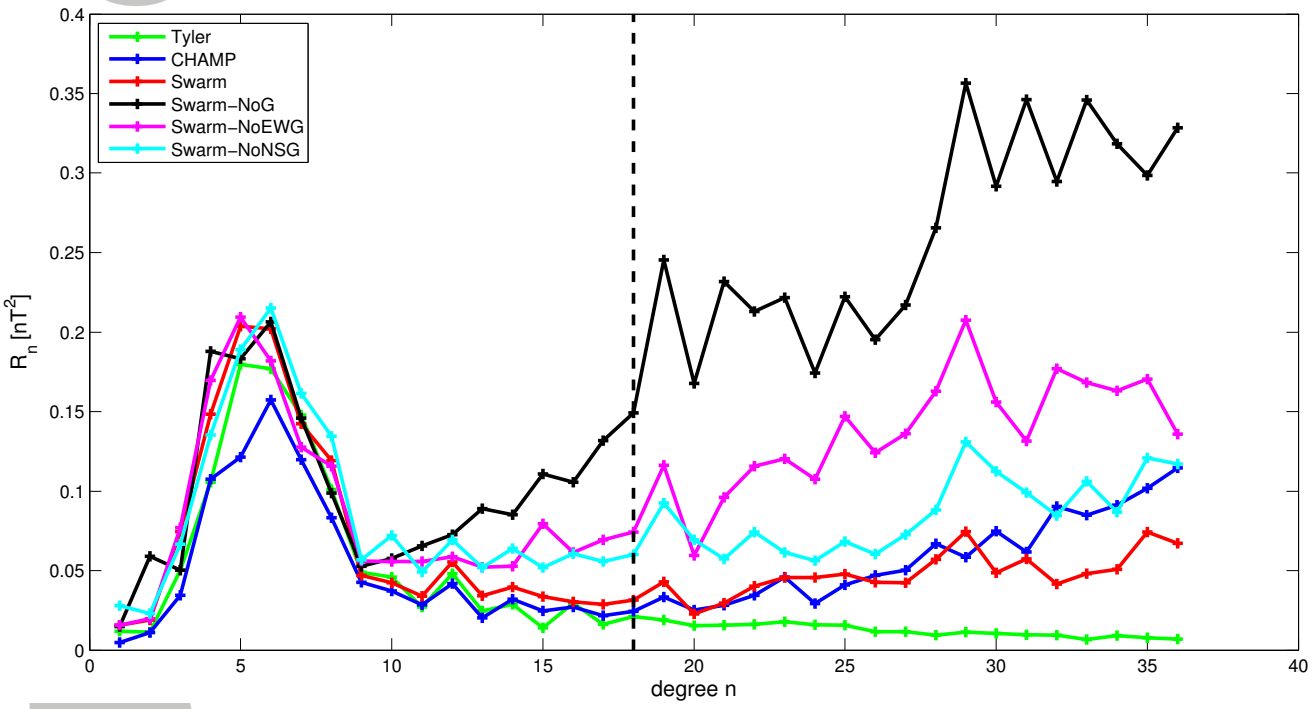

Figure 1. The R_n spectra [*Lowes*, 1966] of the time-averaged oceanic M_2 tidal magnetic field at Earth's mean surface (r=6371.2 km) from n=1−36 for the theoretical forward model of Tyler (green), the estimate from CHAMP (blue), and the estimates from *Swarm* using full gradiometry (red), no gradiometry ("NoG", black), no east-west gradients ("NoEWG", magenta), and no north-south gradients ("NoNSG", cyan). The vertical dashed line at n=18 shows the point above which the CHAMP and full-gradiometry *Swarm* spectra begin to diverge from the theoretical model.

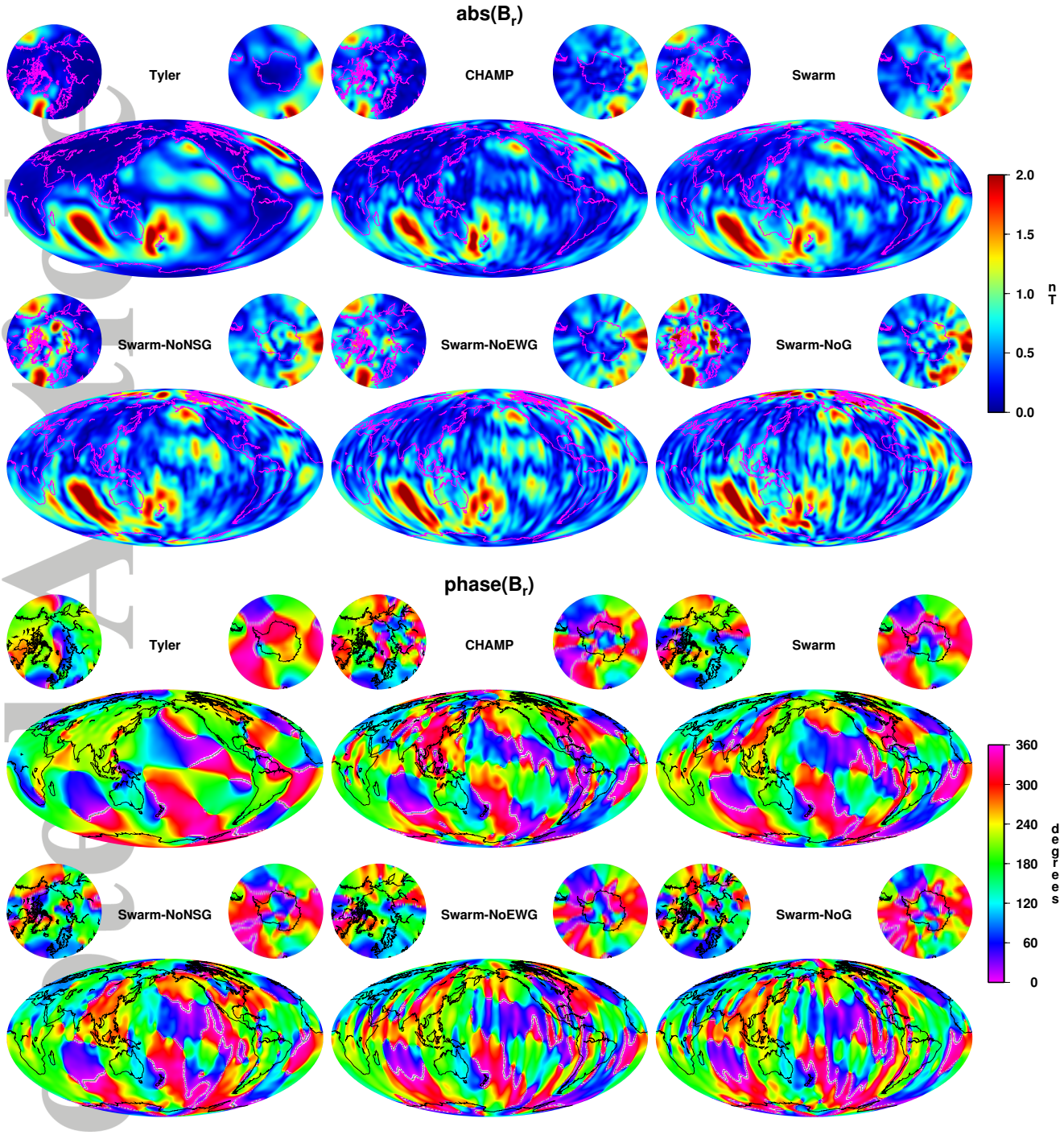

Figure 2. The amplitude (top two rows) and Greenwich phase (bottom two rows) of the B_r component of the oceanic M_2 tidal magnetic field at 430 km altitude computed from the theoretical forward model of Tyler, the estimate from CHAMP, and the estimates from *Swarm* using full gradiometry, no north-south gradients ("NoNSG"), no east-west gradients ("NoEWG"), and no gradiometry ("NoG") for n=1−36.

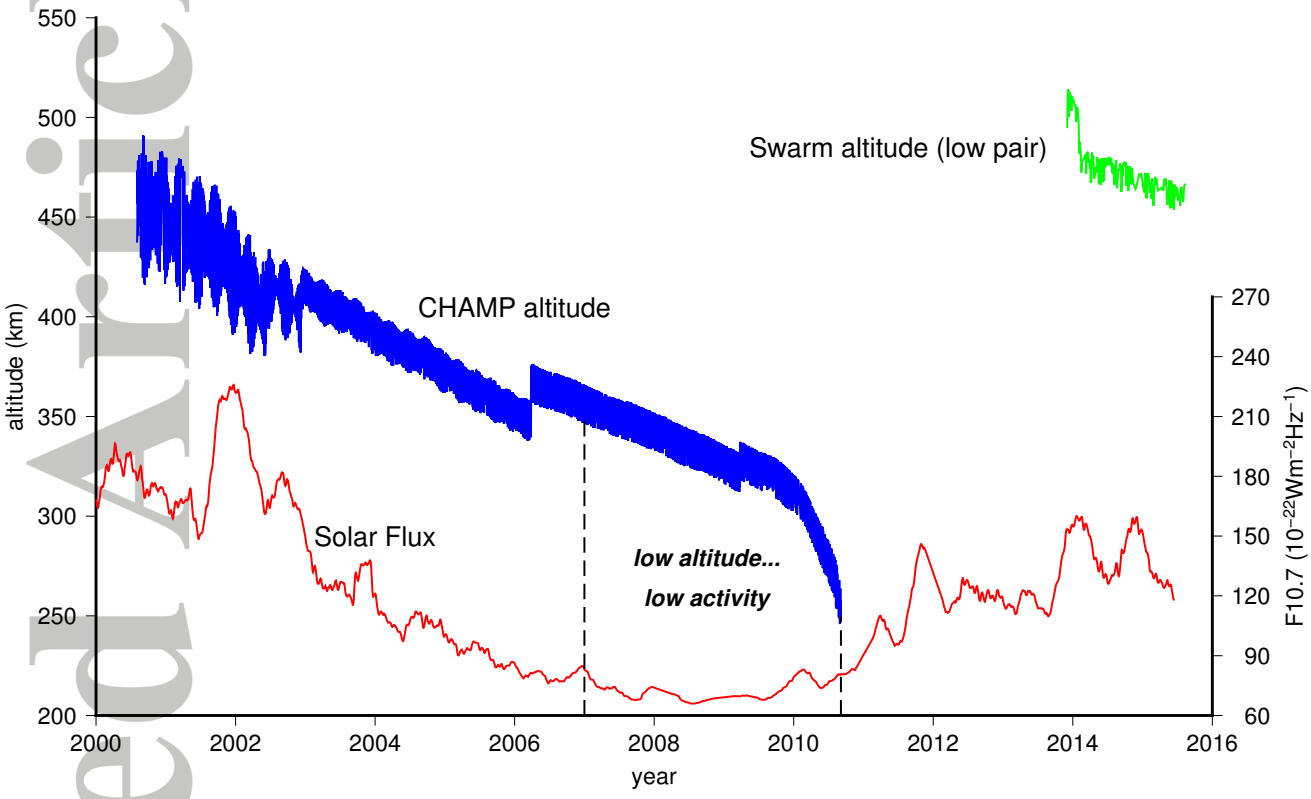

Figure 3. The altitude of CHAMP (blue) and the mean-altitude of the *Swarm* low-pair (green) as indicated by the left scale, and the $F_{10.7}$ solar radiation index (red) as indicated by the right scale. The vertical dashed lines delineate the approximate window of low-altitude and low solar activity during the CHAMP mission.

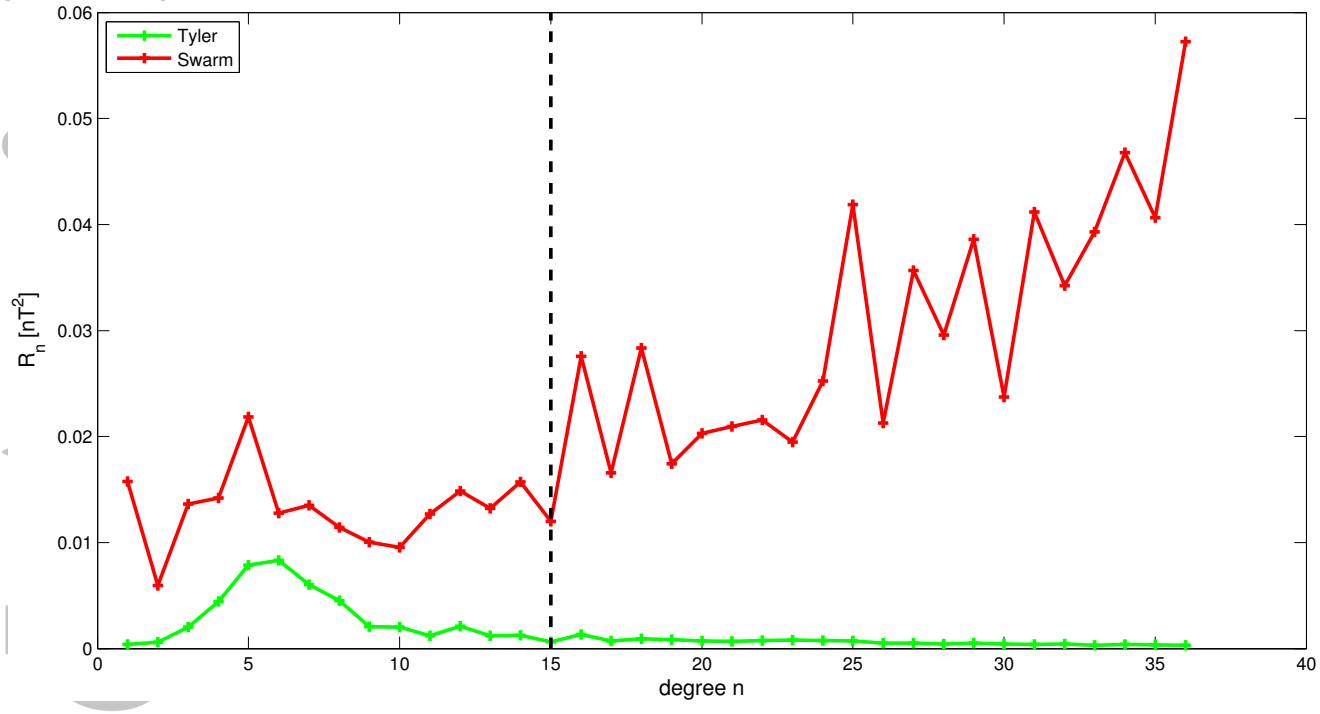

Figure 4. The R_n spectra [*Lowes*, 1966] of the time-averaged oceanic N_2 tidal magnetic field at Earth's mean surface (r=6371.2 km) from n=1−36 for the theoretical forward model of Tyler (green) and the estimate from *Swarm* using full gradiometry (red). The vertical dashed line at n=15 shows the point above which the full-gradiometry *Swarm* spectrum begin to diverge from the theoretical model.

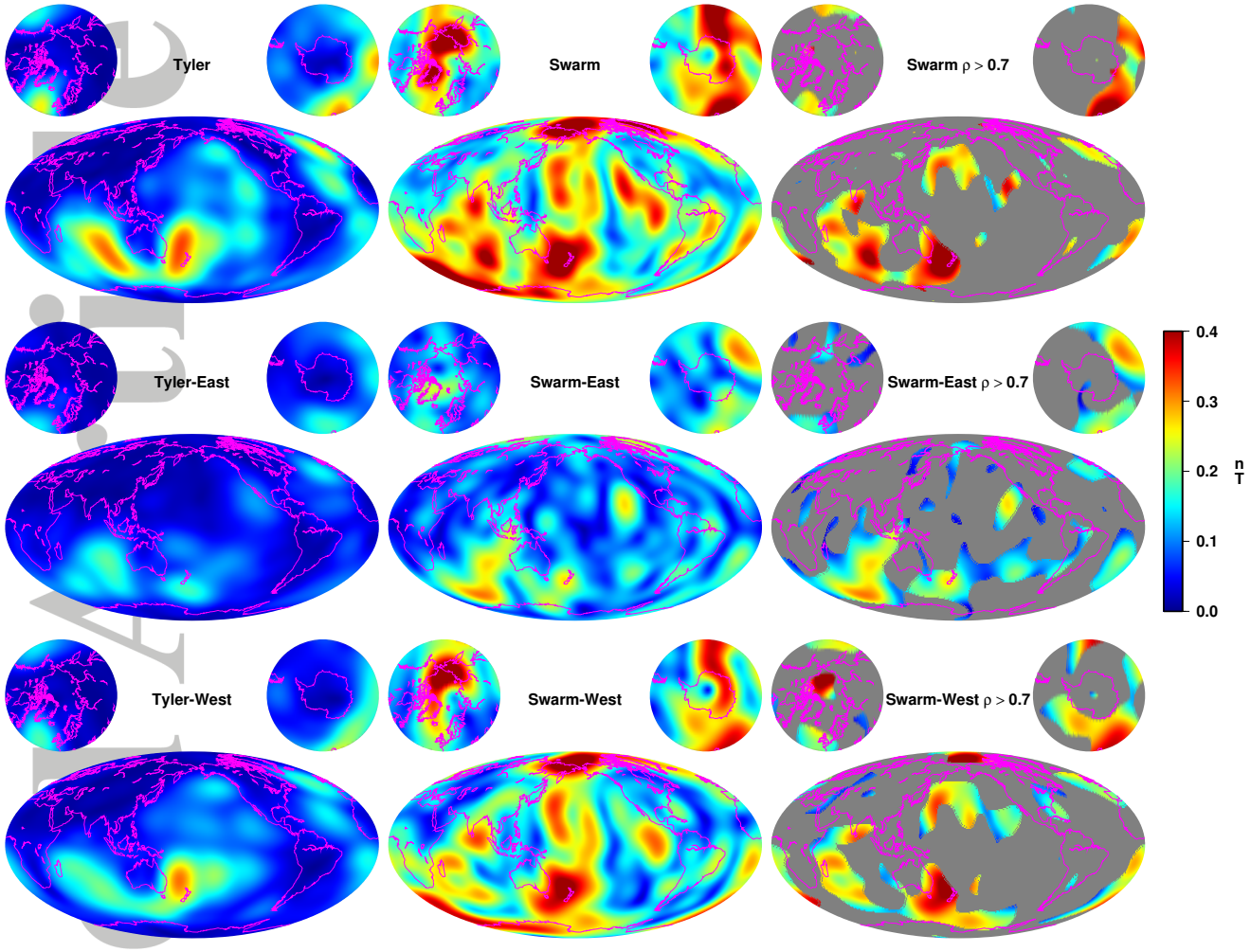

Figure 5. The time-averaged magnitude of the oceanic N_2 tidal magnetic field for n=1−15 (top row), its eastward propagating modes (middle row), and its westward propagating modes (bottom row), at 430 km altitude computed from the theoretical forward model of Tyler (left column), the estimate from *Swarm* using full gradiometry (middle column), and the *Swarm* estimate shown only for regions in which its time-averaged correlations, ρ, with the theoretical model are above 0.7 (right column). The color scale saturates at 0.4 nT.